photonics

MDPI

Review

A Mini-Review: Cooperative Spontaneous Emission from Two- and Three-Level Atoms

Munkh-Uchral Bazarsan [1,2], Mend-Amar Lutsukh [1,2], Tuguldur Begzjav [2] and Gombojav O. Ariunbold [3,4,5,*]

[1] Institute of Physics and Technology, Mongolian Academy of Sciences, Ulaanbaatar 13330, Mongolia
[2] Department of Physics, National University of Mongolia, Ulaanbaatar 14200, Mongolia
[3] Department of Physics and Astronomy, Mississippi State University, Mississippi State, MS 39762, USA
[4] Physics Department, Wesleyan University, Middletown, CT 06459, USA
[5] Department of Physics and Astronomy, Texas A&M University, College Station, TX 77843, USA
* Correspondence: ag2372@msstate.edu

Abstract

In Dicke superradiance, N identical two-level atoms in a small volume share one collective excitation ladder, and the ensemble discharges in a delayed burst whose peak grows in accordance with N^2 rather than N. Real emitters, however, usually have more than two levels. When such an ensemble radiates cooperatively, its multiple decay channels interact rather than simply add up. This mini-review covers recent work that solves this interaction exactly for three-level atoms. We first recall the two-level benchmark: its exact delay statistics, their Gumbel-distributed fluctuation, and the resulting 21.7% deficit of the ensemble-averaged peak below the semi-classical estimate. The master-equation framework developed by Agarwal and Cho, Kurnit and Gilmore, on which the three-level results rest, comes next. The main part surveys three published papers, one for each of the three dipole-allowed three-level configurations. In the cascade, two emission pulses are correlated through an inherited timing. In the shared-source configuration, two channels compete for one atomic reservoir; for equal rates, as shown by Holzinger et al., this competition produces an exactly uniform terminal distribution, as in a Pólya urn. In the shared-sink configuration, two dynamically independent groups of atoms merge exactly into a single collective burst of the combined ensemble. We call this superradiant synthesis.

Keywords: Dicke superradiance; collective spontaneous emission; three-level atoms; cooperative decay; Pauli master equation; two-mode superradiance

1. Introduction

1.1. What This Mini-Review Is About

Leave an excited atom alone in the vacuum, and it decays exponentially, regardless of whether other excited atoms are nearby. Dicke showed in 1954 [1] that this picture breaks down once the atoms are close enough to share the same radiation field. The vacuum then couples the atoms, and instead of N independent emitters, the ensemble behaves as one quantum system, with its own ladder of collective states. An initially inverted sample discharges in a single burst that is *delayed*, *short*, and *intense*, with a peak power proportional to N^2 rather than N. The effect is called superradiance when the sample starts with a macroscopic dipole and superfluorescence when the dipole builds up from vacuum noise. It has been studied extensively ever since [2–10], and it was confirmed experimentally within two decades of its discovery [11].

Check for updates

Received: 25 August 2026
Revised: 21 September 2026
Accepted: 28 September 2026
Published: 30 September 2026

Copyright: © 2026 by the authors. Licensee MDPI, Basel, Switzerland. This article is an open access article distributed under the terms and conditions of the Creative Commons Attribution (CC BY) license.

Almost all of this founding work treats atoms with only two internal levels, and the reason is technical. A symmetrically prepared ensemble of N identical two-level atoms has only $N+1$ collective states available. What looks at first like an intractable 2^N-dimensional many-body problem collapses into a one-dimensional random walk. Real emitters, though, are rarely two-level systems. A rare-earth ion, an alkali atom, a perovskite nanocrystal, and a color centre each have several allowed optical transitions, not one. When such an ensemble radiates cooperatively, its transitions do not simply add up. They interact through the atomic populations they share, and how they interact depends on how the transitions are connected. The multi-level version of the Dicke master equation was established in the 1970s by Agarwal [12,13]; Agarwal and Trivedi [14]; and Cho, Kurnit and Gilmore [15,16]. That work built on the atomic coherent-state methods developed by Arecchi et al. [17]. To our knowledge, what was still missing almost five decades later was an exact solution for a specific and complete set of few-level wiring patterns. This work set up the multi-level master equation and solved it only approximately for particular configurations (mean-field or noise-free Langevin equations) [14,15], but it did not give exact, mode-resolved timing statistics (the delay of each emission mode and its fluctuation) for each dipole-allowed three-level configuration; these, together with the running delay and fluctuation of Equation (5) [18], are what the papers reviewed here add.

Here, we review work that fills this gap for atoms with three internal levels. We do not re-derive the results. Our aim is to set five papers (three published, two posted on the arXiv) side by side and to connect them to the classic and early literature they build on. Two-level Dicke superradiance comes first, since every multi-level result that follows is measured against it. Three-level atoms have three dipole-allowed wiring patterns. In a *cascade* (ladder), the atom descends through two transitions in sequence [18]. When the two transitions share an upper level (the Λ configuration), they compete for one atomic reservoir and can be tuned against each other [19]; when they share a lower level (the V configuration), two initially separate groups of atoms merge into a single collective burst [20]. Below, we call the Λ and V configurations *shared-source* and *shared-sink* because these names state directly which level the two channels share. Two companion papers go further, and we cite both throughout. One gives closed-form (Bateman-type) solutions, i.e., sums of exponentials of the kind Bateman obtained for radioactive decay chains [21], for every atomic population in all three three-level wiring patterns at once [22]. The other extends the same master-equation approach from three levels to four and treats all seven dipole-allowed four-level wiring patterns with a single rate equation [23]. We use plain terms such as "two-level atoms" and "three-level atoms" instead of the group-theoretic labels SU(2) and SU(3), except when a result cannot be stated precisely without them.

1.2. Why Now?

We can see two reasons for writing this survey now. One is experimental: cooperative emission is no longer confined to the dilute-gas laboratory; it now appears in a wide range of condensed-matter and cold-atom platforms. Examples include room-temperature superradiance from single diamond nanocrystals [24] and superfluorescence from lead–halide perovskite quantum-dot superlattices [25] and from hybrid perovskite films at high temperatures (even room temperature) [26–29]. It has also been seen in steady-state superradiant lasing with less than one photon in the cavity [30], in the millihertz strontium clock transition [31], and in superradiant bursts from ordered atomic arrays [32,33]. Superradiant bursts have also been observed in a cascaded (chiral) quantum system of atoms coupled with an optical nanofibre [34], and the emergence of second-order coherence during superradiant and superfluorescent emission has recently been measured [35,36]. Collective emission also underlies superradiant phase transitions, ranging from the cavity

experiments of Baumann et al. [37] to a non-equilibrium superradiant phase transition in free space [38]; these driven, steady-state phenomena are outside the scope of this review.

Closest to the cascade case are two other sets of experiments: macroscopic coherence formed under incoherent pumping, together with *cascade* superfluorescence, in rare-earth-doped crystals [39,40], and picosecond- and femtosecond-pumped superfluorescence in alkali vapors [41–46]. The Er:YLF experiments produce a *pair* of correlated bursts from a three-level cascade, and the theory in Section 4 has to account for that.

The other reason is conceptual. Collective decay can be understood as probability flow among the joint occupation states of the atoms, and once it is understood this way, the natural question changes. It is no longer "what does superradiance look like?" but "what does a given pattern of decay channels do?" A cascade correlates two pulses; a shared-source configuration makes two channels compete; and a shared-sink configuration lets one channel donate collective enhancement to the other. Three-level atoms are the smallest system in which this question has a nontrivial answer. The electric-dipole selection rule permits exactly three non-equivalent wiring patterns for a three-level atom, so the answer can be given for every case: one paper, one configuration. This completeness is why we read the three papers reviewed here as one trilogy rather than three separate results.

1.3. Scope

This mini-review covers two-level Dicke superradiance and the three dipole-allowed three-level configurations: the cascade, the shared-source configuration, and the shared-sink configuration [18–20]. We state results; we do not re-derive them. We also summarize the master-equation framework behind all three papers, following Agarwal [12,13] and Cho, Kurnit, and Gilmore [15]. To keep the review short, two closely related papers are cited but not covered in detail: a time-resolved, channel-by-channel account of the dynamics of every three-level configuration [22], and the extension of the same master-equation program from three levels to four [23]. Full derivations, worked examples, numerical checks, and experimental context for every result summarized here are in the original papers. Our purpose is narrower: to state what each paper established, and to show how the five results relate to one another and to the founding two-level theory developed by Dicke, Agarwal, and Cho. This review is therefore focused on one exactly solvable line of work rather than on the whole field of cooperative emission.

All results reviewed here were obtained in the small-sample, permutation-symmetric (Dicke) limit, in which every atom couples identically to the radiation field. Real extended ensembles depart from this limit: resonant dipole–dipole interactions produce collective frequency shifts and can break permutation symmetry; spatially dependent couplings and the sample geometry select preferred emission directions; and in optically thick media, propagation effects reshape the pulses [7,8,32,47]. These effects are an important part of modern superradiance physics and are not treated here. The exact results below should therefore be read as a small-sample benchmark, not as quantitative predictions for extended media; in particular, the comparison with the Er:YLF cascade experiments in Section 4.1 is qualitative, and a quantitative test would require accounting for propagation in the extended crystal.

1.4. Organization of This Mini-Review

Section 2 recalls the two-level benchmark: the collective jump operator; the Pauli-type master equation of Bonifacio, Schwendimann, and Haake [3,4]; the exact delay statistics of Lee [48,49]; and the Gumbel form of their fluctuation. Section 3 summarizes the shared framework (occupation states, collective operators, and the Pauli-type rate equation) on which the three-level results are built. The core of this review is Section 4, which ad-

dresses the cascade, shared-source, and shared-sink configurations in turn; states the main result of each published paper; and compares the result with the two-level benchmark. Section 5 closes with a short synthesis and points ahead to the edge-flux (bond-by-bond flow, Section 3) and four-level extensions.

2. The Two-Level Benchmark

We begin with the two-level case, which supplies the reference numbers for Section 4.

2.1. From One Atom to N Atoms

A single two-level atom has an upper state $|1\rangle$, a lower state $|2\rangle$, and a transition frequency ω. It decays into the vacuum at the Einstein rate $\Gamma = \omega^3|d_{12}|^2/(3\pi\varepsilon_0\hbar c^3)$. Now, place N such atoms within a region that is small compared with the wavelength—the small-sample, or Dicke, limit. Every atom then couples to the same field mode with the same phase, so the vacuum cannot tell them apart. In accordance with Dicke's work [1], the N separate lowering operators are replaced by one collective operator, $J_- = \sum_i \sigma_-^{(i)}$. This gives an equation of motion for the atomic density matrix ρ in Lindblad form, the standard form for decay into a memoryless environment:

$$\frac{\mathrm{d}\rho}{\mathrm{d}t} = \frac{\Gamma}{2}\left(2J_-\rho J_+ - J_+J_-\rho - \rho J_+J_-\right). \tag{1}$$

This equation was first written down by Agarwal [12] and Bonifacio, Schwendimann, and Haake [3,4]. Because J_- is a *sum* over atoms, the quadratic terms in Equation (1) contain cross terms $\sigma_-^{(i)}\rho\,\sigma_+^{(j)}$ with $i \neq j$: one atom emits while a different atom absorbs the emitted amplitude. These cross terms are the whole difference between collective and independent decay: without them, Equation (1) would simply describe N atoms decaying on their own.

2.2. The Dicke Ladder and the Pauli Master Equation

The operators J_+, J_-, and $J_z = \frac{1}{2}\sum_i \sigma_z^{(i)}$ obey the same algebra as an angular momentum. An ensemble prepared symmetrically (every atom treated the same way at $t = 0$) therefore stays on a single ladder of $N+1$ collective states for the rest of its evolution: the Dicke ladder $|J, M\rangle$, with $J = N/2$. We relabel these states by occupation numbers, namely, $q_1 = J + M$ (the number of atoms in $|1\rangle$) and $q_2 = J - M$ (the number in $|2\rangle$). In this notation, the action of J_- on these states is

$$J_-|q_1, q_2\rangle = \sqrt{q_1(q_2+1)}\;|q_1 - 1, q_2 + 1\rangle. \tag{2}$$

Of the two factors that set the emission rate, q_1 just counts the atoms that can still emit. The other, $q_2 + 1$, is a bosonic enhancement: the more atoms have already decayed into the collective mode, the faster the remaining atoms are stimulated to follow. This factor drives every burst in this mini-review. A short calculation from Equation (1) shows that the level populations, $P_n = \langle q_1 = n|\rho|q_1 = n\rangle$, obey a closed equation of their own, with no dependence on the off-diagonal (coherence) terms of ρ:

$$\frac{\mathrm{d}P_n}{\mathrm{d}t} = I(n+1)P_{n+1} - I(n)P_n, \qquad I(n) \equiv \Gamma\, n\,(N - n + 1). \tag{3}$$

This is the Pauli-type master equation of Bonifacio, Schwendimann and Haake [3,4]. In Dicke's notation, with $n = J + M$, the rate is $I(n) = \Gamma(J+M)(J-M+1)$; the normalization of Γ used throughout is stated in Remark 1 (Section 3). Equation (3) describes a one-way (pure-death) classical random walk, shown in Figure 1. It is what makes the problem

solvable: both the two-level case here and the multi-level case in Section 3 reduce to ordinary probability theory instead of a brute-force many-body quantum calculation.

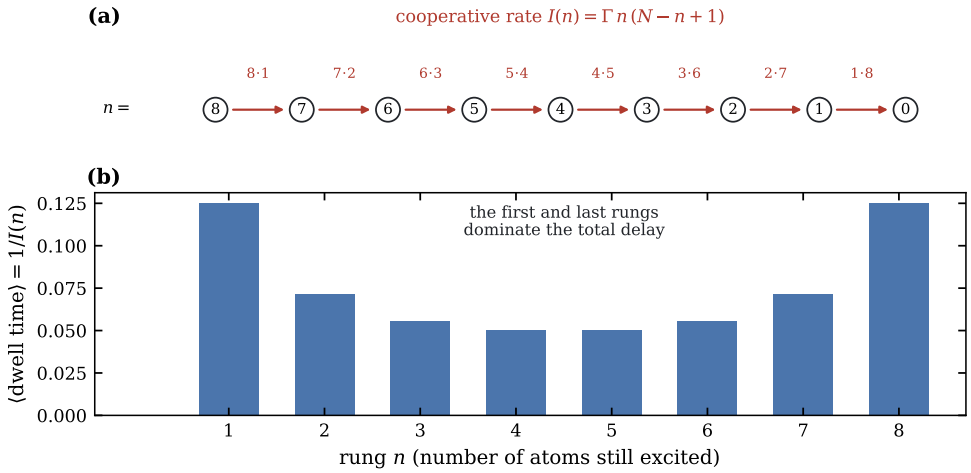


Figure 1. The Dicke ladder as a one-way random walk, with $N = 8$. (**a**) The cooperative rate $I(n) = \Gamma n(N - n + 1)$ is largest in the middle of the chain and smallest at the two ends. (**b**) The mean dwell time $1/I(n)$ on each rung. The delay in the burst is the sum of the dwell times over the upper half of the chain, and this sum is dominated by the first few rungs: the ensemble waits for the first few photons and then avalanches.

2.3. Delay, Fluctuation, and Peak

Equation (3) is a pure-death process, so the waiting time on each rung is exponentially distributed and independent of the waiting times on all other rungs. The time to reach the half-inverted rung is the superradiance delay, τ_D. It is therefore a sum of independent exponential random variables, and its mean and variance are known exactly [48–50] (see Refs. [51,52] for recent analytical treatments of the same master equation):

$$\tau_D = \frac{H_N}{\Gamma(N+1)} = \frac{E_0 + \ln N}{\Gamma N}\left[1 + O(N^{-1})\right], \qquad \frac{\sigma_D}{\tau_D} = \frac{\pi}{\sqrt{6}\,(E_0 + \ln N)}. \tag{4}$$

Here, H_N is the Nth harmonic number, and $E_0 = 0.5772\ldots$ is the Euler–Mascheroni constant. The relative fluctuation shrinks only logarithmically with N: at $N = 200$, it is still 22% of the delay. Superradiance is a macroscopic effect, yet its timing stays uncertain at the level of single photon-emission events. Lee showed that the rescaled delay converges to a Gumbel distribution [53,54], the standard statistical law for the maximum (or, here, the last) of many random events: $\mathrm{Prob}(\Gamma N \tau_D - \ln N \le x) \to \exp(-e^{-x})$. Rényi's representation [55], which writes the maximum of N independent unit exponential variables as the sum $\sum_{k=1}^{N} \mathcal{E}_k/k$ of independent unit exponentials $\mathcal{E}_k$ weighted by $1/k$, makes this result precise, because for a large N, the delay τ_D is dominated by terms of exactly this form. The same fluctuation was measured by Vrehen and co-workers [56,57] and by Crubellier et al. [58]. If one averages the familiar semi-classical sech^2 pulse shape [8,9] over this Gumbel-distributed delay, the ensemble-averaged peak comes out to $\approx 0.1957\, N^2\Gamma$, not the textbook value $N^2\Gamma/4$. The 21.7% reduction comes from the random timing alone: averaging copies of the same pulse shifted by random delays can only lower the peak. Figure 2 collects these benchmarks, against which every three-level result in Section 4 is measured.

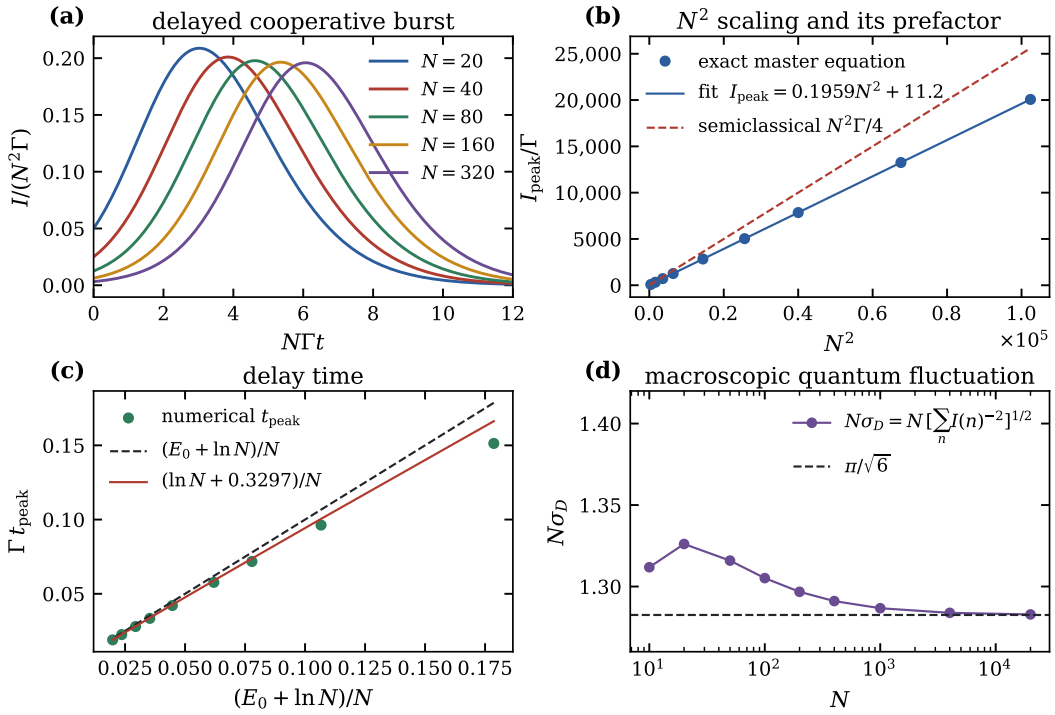


Figure 2. The two-level benchmarks. (**a**) Normalized bursts: rescaling time by $N\Gamma$ collapses the curves, except for the slow logarithmic drift of the delay. (**b**) Peak intensity against N^2, which is about 21.7% below the semiclassical dashed line $N^2\Gamma/4$. (**c**) The time of the peak (dots), compared with the mean delay $(E_0 + \ln N)/(\Gamma N)$ (dashed) and with $(\ln N + 0.3297)/(\Gamma N)$ (solid), the peak time of the Gumbel-averaged sech^2 pulse. The peak comes earlier than the mean delay because the averaged pulse peaks between the most probable delay, $\ln N/(\Gamma N)$, and the mean delay. (**d**) The exact delay standard deviation, rescaled by N, approaching $\pi/\sqrt{6}$.

Section 4 also makes repeated use of the running, or time-dependent, delay and fluctuation, defined at every instant t rather than only at the end of the burst:

$$\langle A(t)\rangle = \int_0^t I(t')\mathrm{d}t', \quad \langle \tau(t)\rangle = \frac{1}{\langle A(t)\rangle}\int_0^t t' I(t')\mathrm{d}t', \quad \langle \sigma(t)\rangle = \frac{\sqrt{\langle \tau^2(t)\rangle - \langle \tau(t)\rangle^2}}{\langle \tau(t)\rangle}. \quad (5)$$

These running observables were introduced in Ref. [18]. Because they are defined at every instant rather than as one number at the end, they show *when*, not just whether, a given emission mode acquires its characteristic timing. This matters most when there are two emission modes, as in Section 4. The three quantities are the cumulative moments of the emitted intensity: $\langle A(t)\rangle$ is the energy radiated up to time t, $\langle \tau(t)\rangle$ is the intensity-weighted mean emission time of the light emitted so far, and $\langle \sigma(t)\rangle$ is its relative spread. They need only the shot-averaged, time-resolved intensity of each emission mode, which can be recorded with a streak camera or time-correlated photon counting after spectral separation of the modes; no photon-correlation measurement is required. At early points in time, when $\langle A(t)\rangle$ is still small, $\langle \sigma(t)\rangle$ is sensitive to detector noise and background, so in practice it is meaningful only once $\langle A(t)\rangle$ exceeds the noise floor. To our knowledge, these running observables have not yet been measured.

3. The Multi-Level Framework

All the three-level results in Section 4 rest on one framework, established by Agarwal [12,13]; Agarwal and Trivedi [14]; and Cho, Kurnit, and Gilmore [15,16]. It applies to atoms with an arbitrary number d of internal levels $|1\rangle, \ldots, |d\rangle$ (with energies $E_1 > \cdots > E_d$), confined to a region that is small compared with every emission wave-

length. We call an allowed transition $|u\rangle \to |l\rangle$ a *channel* (u, l), with Einstein rate Γ_{ul} and photon energy $\hbar\omega_{ul}$. A *configuration* is the set of channels that the atom's selection rules leave open.

Because the atoms are identical and couple identically to the field, an ensemble prepared symmetrically stays symmetric for all time. The relevant states are then the occupation-number states $|\mathbf{q}\rangle = |q_1, \ldots, q_d\rangle$, with $\sum_i q_i = N$: one state for every way of distributing N indistinguishable atoms among d levels. There are $D_N^{(d)} = \binom{N+d-1}{d-1}$ such states. For $d = 3$ and $N = 200$, this is 20 301 states, which can be compared with $3^{200} \approx 10^{95}$ states in the full many-body space. This reduction turns an intractable problem into a sparse system of ordinary differential equations of manageable size. The collective transition operators $A_{nm} = \sum_i |n\rangle_i\langle m|_i$ act on this reduced space in exactly the same way bosonic operators do:

$$A_{nm}|\mathbf{q}\rangle = \sqrt{q_m(q_n + 1)}\; |\mathbf{q} - \mathbf{e}_m + \mathbf{e}_n\rangle. \tag{6}$$

Here, $n, m \in \{1, \ldots, d\}$ label the atomic levels, and $\mathbf{e}_n$ is the unit vector in the q_n direction. Equation (6) generalizes Equation (2) directly to d levels. As before, the first factor counts how many atoms can emit, and the second is the bosonic enhancement from the receiving level. This second factor is the whole mechanism by which one decay channel of a multi-level atom can influence another: a channel that fills level n automatically enhances every other channel that also ends on level n.

Assign one Lindblad decay term to each open channel. Taking the diagonal matrix elements $p(\mathbf{q}, t) = \langle\mathbf{q}|\rho(t)|\mathbf{q}\rangle$ then gives, without approximation, the Pauli-type rate equation

$$\frac{\partial p(\mathbf{q}, t)}{\partial t} = \sum_{(u,l)} \Gamma_{ul}\Big[q_l(q_u + 1)\, p(\mathbf{q} + \mathbf{e}_u - \mathbf{e}_l, t) - q_u(q_l + 1)\, p(\mathbf{q}, t)\Big], \tag{7}$$

with any term that would require a negative occupation number dropped and with total probability $\sum_{\mathbf{q}} p(\mathbf{q}, t) = 1$ conserved. It is the multi-level counterpart of Equation (3), and every paper in Section 4 relies on three of its properties. First, a specific configuration is selected just by setting the corresponding rates to zero; nothing has to be re-derived. Second, Equation (7) describes a classical random walk on a finite, directed graph, so standard tools for first-passage times and occupation times apply directly. Third, every transition strictly lowers the atom's total internal energy, so the graph has no closed loops; ordering the states by energy makes the generator matrix triangular. Weighting each channel's rate by its photon energy gives the total radiated intensity,

$$I(t) = \sum_{(u,l)} \hbar\omega_{ul}\, \Gamma_{ul} \sum_{\mathbf{q}} p(\mathbf{q}, t)\, q_u(q_l + 1), \tag{8}$$

which obeys an exact energy-balance relation, $\mathrm{d}\langle E\rangle/\mathrm{d}t = -I(t)$, for every configuration and every initial condition. The papers reviewed here use this identity throughout to check both analytic and numerical results.

Geometrically, the occupation states $|\mathbf{q}\rangle$ sit at the lattice points of a $(d-1)$-dimensional simplex: a chain of $N + 1$ sites for two-level atoms, and a triangle of $\frac{1}{2}(N + 1)(N + 2)$ sites for three-level atoms (Figure 3). Each open channel moves the state by one fixed step on this lattice, so collective decay is directed probability flow on a lattice. Section 4 traces where this flow goes in each of the three three-level configurations. Reference [22] gives a closed-form, channel-by-channel account of this flow for all three configurations at once: it assigns an exact, time-dependent value to the flow through every lattice bond (the edge flux), not only the total intensity of Equation (8). We only cite this result here. The rate-equation approach

also works beyond three levels. For four-level atoms, the occupation lattice becomes a tetrahedron, and all seven dipole-allowed configurations reduce to one Pauli-type rate equation of the same form as Equation (7). The closed-form transition matrix elements and the emitted intensity for that case are worked out in Ref. [23].

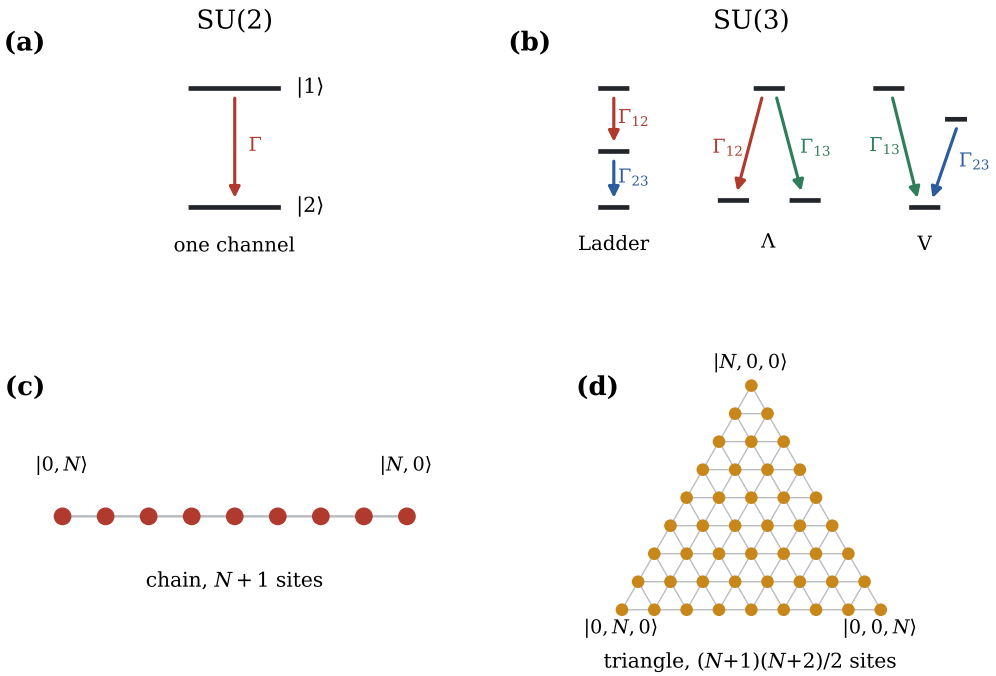


Figure 3. (**a**) The two-level atom and its single channel. (**b**) The three dipole-allowed three-level configurations covered in Section 4: cascade, shared-source, and shared-sink. (**c**,**d**) The corresponding occupation-number lattices at $N = 8$: a chain of $N + 1$ sites and a triangle of $\frac{1}{2}(N + 1)(N + 2)$ sites. Four-level atoms occupy a tetrahedron [23].

Remark 1 (Normalization)**.** *We use the convention in which* Γ_{ul} *is the ordinary Einstein A coefficient, so a single isolated atom in* $|u\rangle$ *decays at rate* Γ_{ul}*. Some of the literature, including Ref. [23], instead defines a rate* γ_{lu} *with a unit prefactor in the decay term; the two conventions are related by* $\Gamma_{ul} = 2\gamma_{lu}$*. This choice affects only absolute rate prefactors, not exponents, delays, or pulse shapes.*

4. Three-Level Atoms: A Trilogy of Configurations

The electric-dipole selection rule restricts a three-level atom to exactly three inequivalent maximal channel configurations, each with two open channels. They are the *cascade* ($1 \to 2, 2 \to 3$); the *shared-source* configuration, in which one upper level feeds two lower ones ($1 \to 2, 1 \to 3$, conventionally labeled Λ); and the *shared-sink* configuration, in which two upper levels feed one common lower level ($1 \to 3, 2 \to 3$; conventionally labeled V). This count of three follows from a parity argument. The dipole operator is parity-odd, so each level carries a parity label, and a channel is open only between two levels of opposite parity. With three levels, there are only two parity classes, so at least one pair of levels must share a parity; the channel between that pair is closed. Which pair is closed fixes the configuration (Figure 4). The same argument gives $2^{d-1} - 1$ maximal configurations for a general d-level atom: one for two levels, three for three levels, and seven for four levels. The four-level case is the subject of Ref. [23].

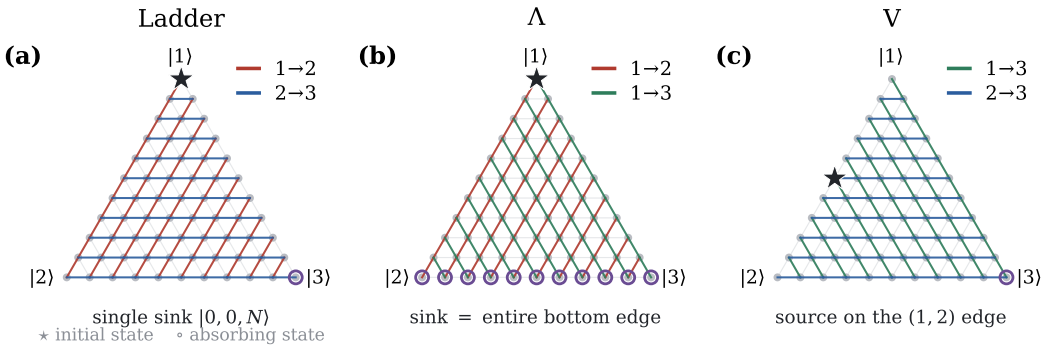


Figure 4. The three dipole-allowed three-level configurations as bond sets on the triangular occupation-number lattice ($N = 10$). Grey bonds are lattice directions closed by parity; colored bonds are open channels. Stars mark the initial states used in each paper reviewed below; open circles mark absorbing states (states the ensemble cannot leave). (**a**) Cascade: The two channels are in series, and the flow must cross the lattice from $|N, 0, 0\rangle$ to $|0, 0, N\rangle$. (**b**) Shared-source: The two channels compete for the same source, and the absorbing set is the entire bottom edge. (**c**) Shared-sink: The natural initial state is the midpoint of the $(1, 2)$ edge, and both channels end on the same vertex.

Even before any equations are solved, the three configurations differ qualitatively. The cascade's two channels act *in series*: the decay must pass through the whole lattice, one step at a time. In the shared-source configuration, they act in parallel and *compete* for the same upper level, so which lower level each atom ends up in is decided stochastically, not set in advance. The shared-sink channels are parallel too, but there, they *cooperate* because both feed the same lower level. Each of the next three subsections reviews the paper that works out one of these cases in full.

4.1. Cascade: Correlated Pulse Pairs

For the cascade, Equation (7) couples channels $(1, 2)$ and $(2, 3)$. Reference [18] solves this system exactly, starting from full inversion, $p(N, 0, 0) = 1$, and characterizes it by the rate ratio $\alpha = \Gamma_{23}/\Gamma_{12}$. The paper's central finding is that the ensemble emits a *correlated pair* of bursts, not two independent ones. The upper transition behaves like an ordinary two-level burst: its delay, $\tau_{1D} = (E_0 + \ln N)/(\Gamma_{12} N)$, is essentially unaffected by the second channel as long as $\alpha \lesssim 0.1$. The lower transition is the interesting one: it cannot begin until level 2 has been populated, and this population comes directly from the upper transition. Its delay therefore *adds* to the first transition's delay, $\langle \tau_2(\infty) \rangle \simeq \tau_{1D} + \tau_{2D}$, with $\tau_{2D} \simeq \tau_{1D}/\alpha$. Both modes retain the N^2 scaling of the two-level benchmark. Its main methodological contribution is the running fluctuation $\langle \sigma(t) \rangle$ of Equation (5). The first mode's running fluctuation has a single minimum, located at its own delay. The second mode's running fluctuation has *two*: an early one inherited from the first mode's timing, and a later one of its own (Figure 5d). This two-minimum signature gives a sharper test of correlation between the two pulses than a static delay measurement for a simple reason. A single delay number cannot tell "late because slow" apart from "late because it had to wait"; the running fluctuation can. Er:YLF cascade measurements [39,40] report this kind of correlated pulse pair, with a reproducible relative delay consistent with $\tau_{1D} + \tau_{2D}$. The two-minimum structure of the running fluctuation is a more specific prediction of Ref. [18], and, to our knowledge, it has not yet been tested experimentally. Testing it requires only the shot-averaged, time-resolved intensities of the two spectrally separated cascade pulses (Section 2).

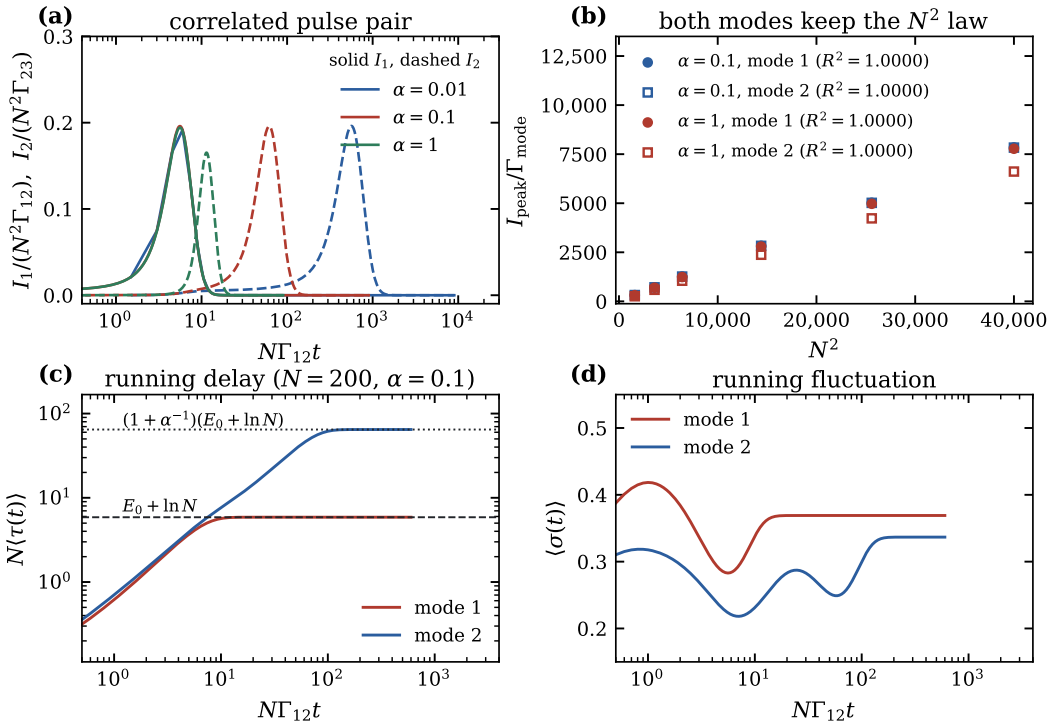


Figure 5. Cascade superradiance, as per Ref. [18]. (**a**) Mode-resolved transients for $N = 200$: decreasing α separates the pulse pair in time without changing either pulse's shape. (**b**) Both modes obey the N^2 law. (**c**) Running delays: Mode 1 saturates at $E_0 + \ln N$ and mode 2 at $(1+\alpha^{-1})(E_0 + \ln N)$. (**d**) Running fluctuations: Mode 2's two minima are the timing signature of a correlated pulse pair.

4.2. Shared Source: Competition and Mode-Selective Control

In the shared-source (Λ) configuration, channels $(1,2)$ and $(1,3)$ both drain the same upper level. Reference [19] solves this case, again from full inversion, with a rate ratio $\alpha = \Gamma_{13}/\Gamma_{12}$. Its main result is mode-selective control, as discussed below. The final distribution of atoms between the two lower levels is not treated in Ref. [19]; it has been obtained exactly by Holzinger et al. [59], whose work is summarized below. For equal rates, $\alpha = 1$, this distribution is *exactly uniform*, not binomial. Every possible split $k = 0, 1, \ldots, N$ between the two lower levels is equally likely. The proof comes from classic probability theory. At each step, the two channels compete for the next atom, and the probability of each outcome reduces to that of a Pólya urn: an urn that starts with one ball of each color and gains one ball of the color just drawn after every draw [54,60]. The correspondence is exact: after q_2 atoms have decayed through channel $(1,2)$ and q_3 have decayed through channel $(1,3)$, Equation (6) gives the rates $\Gamma q_1(q_2+1)$ and $\Gamma q_1(q_3+1)$, so the next atom takes channel $(1,2)$ with probability $(q_2+1)/(q_2+q_3+2)$. The enhancement factors q_2+1 and q_3+1 are exactly the ball counts of the urn. The exact solution of a Pólya urn is the discrete uniform distribution. Independent branching, atom by atom, would instead give a binomial distribution sharply peaked around an equal split. The bosonic enhancement factor in Equation (6) favors whichever channel is already ahead, and this positive feedback is what flattens the binomial peak into a uniform distribution. For $\alpha \neq 1$, the branching process becomes a Friedman–Bagchi–Pal urn with unequal reinforcement [61,62]. The disadvantaged channel's share of the atoms then vanishes rapidly with N: at $\alpha = 0.1$ and $N = 60$ (Figure 6d), more than 97% of the probability lies within three atoms of complete transfer to the favored channel (about 92% at $N = 1000$).

The shared-source problem has been solved in full by Holzinger et al. [59]. They considered N emitters with one excited state that decays collectively into d ground sublevels and solved the master equation with a symbolic quantum-trajectory method. For $d = 2$,

this is exactly the shared-source configuration reviewed here, with the same normalization of the rates and with their ratio $r = \Gamma_2/\Gamma_1$ playing the role of α. Starting from full inversion, they express every population as a finite sum of exponentials, valid for any N and any rates, and give a closed form for the final distribution over the two ground sublevels for any N and any r (Equation (A5) of Ref. [59]). At $r = 1$, it reduces to the uniform distribution $1/(N+1)$ discussed above, and they connect the problem to a two-color Pólya urn with unequal reinforcement.

Holzinger et al. also show that the mean fraction of atoms that end in the second ground sublevel, $\bar{n}_2$, acts as the order parameter of a dissipative first-order transition at $r = 1$. By symmetry, $\bar{n}_2 = 1/2$ there, and its slope, $\partial_r \bar{n}_2|_{r=1} = (N+2)(H_{N+1} - 1)/(6N) \simeq (\ln N)/6$, diverges logarithmically with N, so for $N \to \infty$, the faster channel collects essentially all the atoms. For d channels of an equal rate, they derive scaling laws for the peak time and peak intensity of the burst. Their results thus cover the final state of the shared-source configuration, while Ref. [19] covers its emitted intensities, delays and mode-selective control.

Mode-selective control, the main result of Ref. [19], works as follows. Mode 1 obeys the N^2 law for every value of α, but its coefficient $s_1(\alpha)$ falls from 0.195 at $\alpha = 0.1$ to 0.111 at $\alpha = 1$, amounting to nearly a factor of two. The change is controlled entirely by the *other* channel's rate; nothing about mode 1's own transition is altered. The cascade offers no such control because there, the second channel cannot influence the first until the second channel starts.

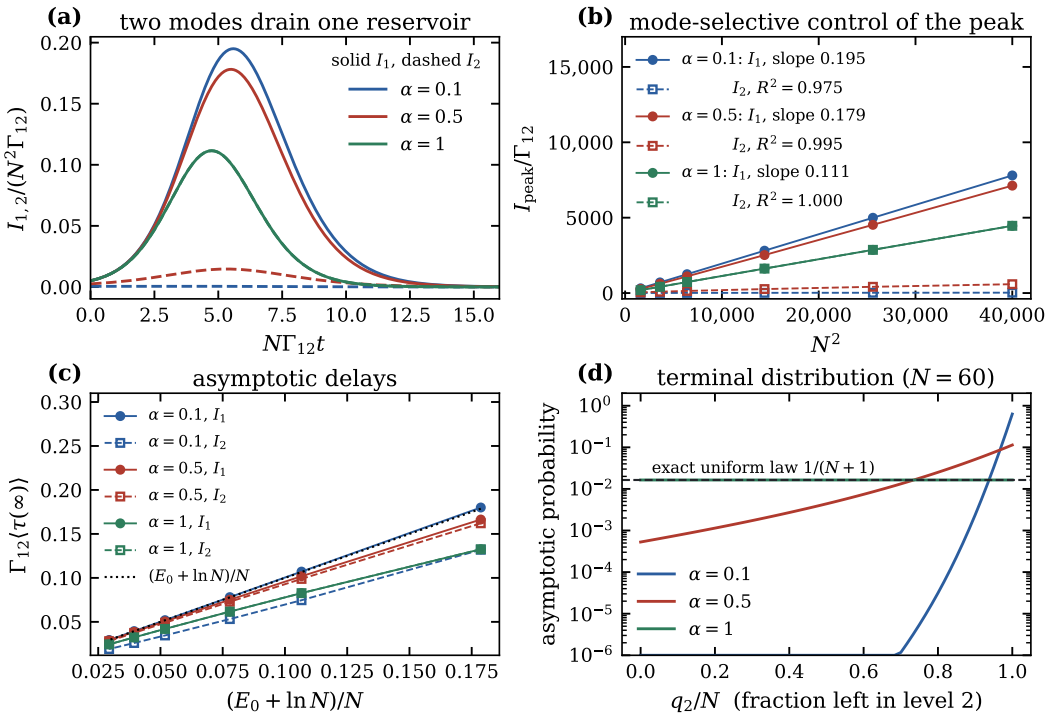


Figure 6. The shared-source configuration; panels (**a**–**c**) correspond to Ref. [19], and panel (**d**) was computed for this review from Equation (7) (cf. Ref. [59]). (**a**) Mode-resolved transients at $N = 200$: The two channels drain one reservoir, so strengthening one weakens the other. (**b**) Peak intensity against N^2: Mode 1's slope falls from 0.195 ($\alpha = 0.1$) to 0.111 ($\alpha = 1$), constituting the mode-selective control effect. (**c**) Asymptotic running delays. (**d**) Final distribution over the absorbing bottom edge: It is exactly uniform at $\alpha = 1$ (dashed line) and increasingly one-sided as α decreases.

4.3. Shared Sink: Superradiant Synthesis

The shared-sink (V) configuration opens channels $(1,3)$ and $(2,3)$: two upper levels both decay to one common lower level. Reference [20] starts from an initial state that is

different from the other two papers: this is not full inversion, but there are N atoms in each excited level and none in the ground level, $p(N, N, 0) = 1$. At $t = 0$, the two groups are dynamically independent, and in isolation, each would undergo its own N-atom two-level burst. The central result is that, for equal rates $\Gamma_{13} = \Gamma_{23} = \Gamma$, the two groups do *not* stay independent. The population of the shared ground level follows exactly the same equation as a two-level Dicke chain for the *combined* $2N$-atom ensemble for every possible initial split between the two excited levels. The paper calls this result superradiant *synthesis*: two groups of atoms that share only a ground level end up radiating exactly as a single combined ensemble. The bosonic enhancement from the shared ground level erases any memory of how the atoms were originally divided between the two excited levels. The mechanism can be gleaned from Equation (7): for equal rates, the total rate at which the ensemble leaves a state $|q_1, q_2, q_3\rangle$ is $\Gamma(q_1 + q_2)(q_3 + 1)$, which depends only on the number $q_1 + q_2 = 2N - q_3$ of excited atoms, not on how they are split. The ground-level population therefore performs exactly the two-level walk of Equation (3) with $N \to 2N$ for any initial split (q_1, q_2) with $q_1 + q_2 = 2N$, not only the symmetric one. For unequal rates, the coupling shows up in the timing. The faster channel bursts first, on its own Dicke schedule, and deposits its atoms in the shared ground level. The slower channel then starts from a population already at the point of the maximum cooperative rate in its own Dicke chain, so it fires with *no* build-up delay. The resulting speed-up scales as follows (Figure 7c): $1 + \Gamma_{13}/\Gamma_{23}$.

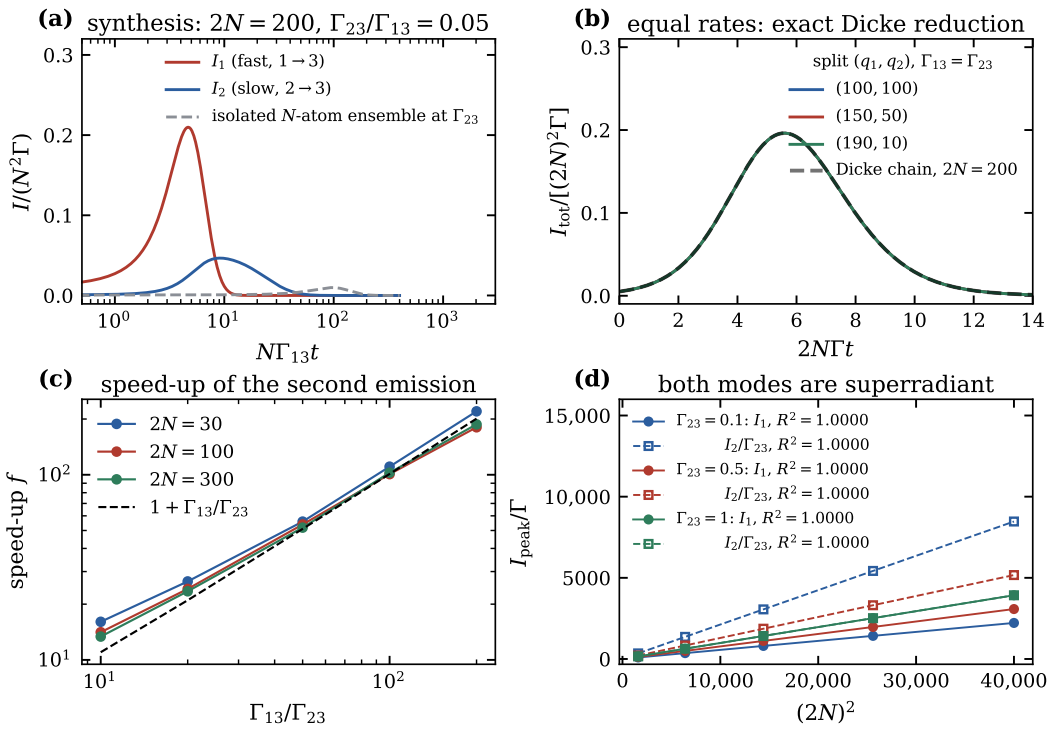


Figure 7. The shared-sink configuration and superradiant synthesis, as per Ref. [20]. (**a**) The slow mode fires immediately behind the fast one, which is an order of magnitude earlier than the same group of atoms would fire in isolation (dashed). (**b**) For equal rates, the total transient is exactly the $2N$-atom two-level burst for every split of the atoms between the two excited levels. (**c**) The speed-up factor against the rate ratio. (**d**) Both modes obey the N^2 law throughout, unlike the shared-source case.

4.4. The Three Configurations Compared

All three papers share one lattice, one master equation, and one matrix element. They differ only in where the bosonic enhancement factor acts. Table 1 summarizes the comparison.

Table 1. The three three-level configurations compared.

	Cascade	**Shared Source**	**Shared Sink**
Reference	[18]	[19]	[20]
Channels	in series	parallel, shared source	parallel, shared sink
Enhancement	inherited	contested	donated
Main effect	correlation	competition	synthesis
Absorbing set	one vertex	one edge	one vertex
Second mode	delayed by $\tau_{1D} + \tau_{2D}$	suppressed if $\alpha \ll 1$	advanced to τ_{1D}
N^2 law, mode 2	holds	degrades	holds
Solvable limit	$\alpha \to 0$: two Dicke edges	$\alpha = 1$: uniform urn [59]	$\Gamma_{13} = \Gamma_{23}$: Dicke chain

Within the small-sample model considered here, these three configurations exhaust the dipole-allowed channel configurations of a three-level atom. A fourth level allows the three effects to be combined, and it also allows configurations whose channel graph contains a closed loop rather than only tree-like branches, which is impossible with three levels. This four-level case is the subject of Ref. [23]. A channel-by-channel account of the flow underlying all three configurations above is given in Ref. [22].

5. Conclusions

Collective spontaneous emission from identical few-level atoms, in the small-sample limit, reduces exactly to directed probability flow on a lattice of occupation states. One operator relation governs that flow, $A_{nm}|\mathbf{q}\rangle = \sqrt{q_m(q_n+1)}|\mathbf{q}'\rangle$. Its bosonic-enhancement factor is the origin of the two-level N^2 burst, and it is also the entire mechanism by which one decay channel of a multi-level atom influences another. The two-level benchmark reviewed in Section 2 sets the standard for every three-level result: the exact delay $\tau_D = H_N/[\Gamma(N+1)]$, its Gumbel-distributed fluctuation, and the resulting $\approx 0.1957\, N^2\Gamma$ ensemble-averaged peak.

The three-level trilogy surveyed in Section 4 shows that the three dipole-allowed configurations of a three-level atom behave in three different ways, even though they share one master equation. In the cascade, the second pulse inherits the timing of the first, a correlation exposed by the two-minimum structure of the running fluctuation [18]. The shared-source channels compete instead: they drain one reservoir, so one mode's peak can be tuned by nearly a factor of two through the *other* mode's rate [19]. For equal rates, the ensemble ends in an exactly uniform distribution over the absorbing edge, constituting a Pólya-urn effect, not the binomial distribution one might expect [59]. The shared-sink configuration, finally, synthesizes. For equal rates, the whole three-level problem collapses exactly onto a two-level Dicke chain of the combined ensemble. For unequal rates, the slower group of atoms is handed a population already at the point of the maximum cooperative rate, and it radiates with no build-up delay [20].

The trilogy belongs to a larger body of work. A companion paper gives an exact, closed-form, channel-by-channel account of every state in every three-level configuration within one framework [22]. The rate-equation approach that unifies the cascade, shared-source, and shared-sink configurations in Equation (7) also extends, without modification, to four-level atoms, where seven dipole-allowed configurations reduce to one Pauli-type equation on a tetrahedral occupation lattice [23]. Historically, the line runs from Dicke's original two-level reduction [1], through the multi-level master equation of Agarwal [12,13] and Cho, Kurnit, and Gilmore [15], to the three-level trilogy reviewed here and its four-level extension. The main lesson of these papers is that the channel *topology* of a few-level atom, not just its level spacings or decay rates, decides how the atom radiates collectively.

Author Contributions: Conceptualization, G.O.A.; writing—original draft preparation, G.O.A., M.-U.B., M.-A.L. and T.B.; writing—review and editing, G.O.A.; supervision, G.O.A. All authors have read and agreed to the published version of the manuscript.

Funding: This research received no external funding.

Data Availability Statement: No new data were created in this study. Data sharing is not applicable to this article.

Acknowledgments: During the preparation of this manuscript, the authors used Claude Opus 5.5 (Anthropic) to assist with condensing and restructuring draft text into review form. The authors have reviewed and edited the output and take full responsibility for the content of this publication.

Conflicts of Interest: The authors declare no conflicts of interest.

References

1. Dicke, R.H. Coherence in spontaneous radiation processes. *Phys. Rev.* **1954**, *93*, 99–110. [CrossRef]
2. Rehler, N.E.; Eberly, J.H. Superradiance. *Phys. Rev. A* **1971**, *3*, 1735–1751. [CrossRef]
3. Bonifacio, R.; Schwendimann, P.; Haake, F. Quantum statistical theory of superradiance. I . *Phys. Rev. A* **1971**, *4*, 302–313. [CrossRef]
4. Bonifacio, R.; Schwendimann, P.; Haake, F. Quantum statistical theory of superradiance. II. *Phys. Rev. A* **1971**, *4*, 854–864. [CrossRef]
5. Degiorgio, V. Statistical properties of superradiant pulses. *Opt. Commun.* **1971**, *2*, 362–364. [CrossRef]
6. Bonifacio, R.; Lugiato, L.A. Cooperative radiation processes in two-level systems: Superfluorescence. *Phys. Rev. A* **1975**, *11*, 1507–1521. [CrossRef]
7. MacGillivray, J.C.; Feld, M.S. Theory of superradiance in an extended, optically thick medium. *Phys. Rev. A* **1976**, *14*, 1169–1189. [CrossRef]
8. Gross, M.; Haroche, S. Superradiance: An essay on the theory of collective spontaneous emission. *Phys. Rep.* **1982**, *93*, 301–396. [CrossRef]
9. Benedict, M.G.; Ermolaev, A.M.; Malyshev, V.A.; Sokolov, I.V.; Trifonov, E.D. *Super-Radiance: Multiatomic Coherent Emission*; CRC Press: Boca Raton, FL, USA, 1996.
10. Andreev, A.V.; Emel'yanov, V.I.; Il'inskii, Y.A. Collective spontaneous emission (Dicke superradiance). *Sov. Phys. Usp.* **1980**, *23*, 493–514. [CrossRef]
11. Skribanowitz, N.; Herman, I.P.; MacGillivray, J.C.; Feld, M.S. Observation of Dicke superradiance in optically pumped HF gas. *Phys. Rev. Lett.* **1973**, *30*, 309–312. [CrossRef]
12. Agarwal, G.S. Master-equation approach to spontaneous emission. *Phys. Rev. A* **1970**, *2*, 2038–2046. [CrossRef]
13. Agarwal, G.S. Quantum statistical theory of coherent emission from a system of multi-level atoms. *Phys. Lett. A* **1973**, *45*, 15–17. [CrossRef]
14. Agarwal, G.S.; Trivedi, S.S. Superradiance from three-level systems in atomic coherent state representation. *Opt. Commun.* **1976**, *18*, 417–420. [CrossRef]
15. Cho, Y.C.; Kurnit, N.A.; Gilmore, R. Superradiance from a system of three-level particles. In *Coherence and Quantum Optics*; Mandel, L., Wolf, E., Eds.; Plenum: New York, NY, USA, 1973; pp. 755–766.
16. Gilmore, R. Coherent states in modern physics. In *Coherence and Quantum Optics*; Mandel, L., Wolf, E., Eds.; Plenum: New York, NY, USA, 1973; p. 217.
17. Arecchi, F.T.; Courtens, E.; Gilmore, R.; Thomas, H. Atomic coherent states in quantum optics. *Phys. Rev. A* **1972**, *6*, 2211–2237. [CrossRef]
18. Ariunbold, G.O. A cascade superradiance model. *Phys. Lett. A* **2022**, *452*, 128468. [CrossRef]
19. Ariunbold, G.O.; Begzjav, T. A mode-selective control in two-mode superradiance from lambda three-level atoms. *Photonics* **2025**, *12*, 674. [CrossRef]
20. Ariunbold, G.O.; Begzjav, T. Superradiant syntheses via the V-type three-level atoms. *Phys. Lett. A* **2026**, *571*, 131299. [CrossRef]
21. Bateman, H. The solution of a system of differential equations occurring in the theory of radioactive transformations. *Proc. Camb. Philos. Soc.* **1910**, *15*, 423–427.
22. Ariunbold, G.O.; Sivaraman, V. Time-resolved edge flux on the SU(3) triangle: A cooperative-decay graph framework with exact Bateman solutions. *arXiv* **2026**, arXiv:2608.22664.
23. Lutsukh, M.-A.; Bazarsan, M.-U.; Begzjav, T.; Ariunbold, G.O. Multi-channel collective dissipation via the fully symmetric irreducible representation of SU(4). *arXiv* **2026**, arXiv:2607.07701.

24. Bradac, C.; Johnsson, M.T.; van Breugel, M.; Baragiola, B.Q.; Martin, R.; Juan, M.L.; Brennen, G.K.; Volz, T. Room-temperature spontaneous superradiance from single diamond nanocrystals. *Nat. Commun.* **2017**, *8*, 1205. [CrossRef]
25. Rainò, G.; Becker, M.A.; Bodnarchuk, M.I.; Mahrt, R.F.; Kovalenko, M.V.; Stöferle, T. Superfluorescence from lead halide perovskite quantum dot superlattices. *Nature* **2018**, *563*, 671–675. [CrossRef]
26. Findik, G.; Biliroglu, M.; Seyitliyev, D.; Mendes, J.; Barrette, A.; Ardekani, H.; Lei, L.; Dong, Q.; So, F.; Gundogdu, K. High-temperature superfluorescence in methyl ammonium lead iodide. *Nat. Photonics* **2021**, *15*, 676–680. [CrossRef]
27. Biliroglu, M.; Findik, G.; Mendes, J.; Seyitliyev, D.; Lei, L.; Dong, Q.; Mehta, Y.; Temnov, V.V.; So, F.; Gundogdu, K. Room-temperature superfluorescence in hybrid perovskites and its origins. *Nat. Photonics* **2022**, *16*, 324–329. Correction in *Nat. Photonics* **2022**, *16*, 396. [CrossRef]
28. Huang, K.; Green, K.K.; Huang, L.; Hallen, H.; Han, G.; Lim, S.F. Room-temperature upconverted superfluorescence in a single lanthanide-doped upconversion nanoparticle. *Nat. Photonics* **2022**, *16*, 737–742.
29. Gundogdu, K.; So, F.; Brongersma, M.L.; Biliroglu, M.; Findik, G. Quantum analog of vibration isolation: From room-temperature superfluorescence to high-temperature superconductivity. *arXiv* **2022**, arXiv:2204.09807.
30. Bohnet, J.G.; Chen, Z.; Weiner, J.M.; Meiser, D.; Holland, M.J.; Thompson, J.K. A steady-state superradiant laser with less than one intracavity photon. *Nature* **2012**, *484*, 78–81. [CrossRef]
31. Norcia, M.A.; Winchester, M.N.; Cline, J.R.K.; Thompson, J.K. Superradiance on the millihertz linewidth strontium clock transition. *Sci. Adv.* **2016**, *2*, e1601231. [CrossRef]
32. Masson, S.J.; Asenjo-Garcia, A. Universality of Dicke superradiance in arrays of quantum emitters. *Nat. Commun.* **2022**, *13*, 2285. [CrossRef]
33. Ferioli, G.; Glicenstein, A.; Robicheaux, F.; Sutherland, R.T.; Browaeys, A.; Ferrier-Barbut, I. Laser-driven superradiant ensembles of two-level atoms near Dicke regime. *Phys. Rev. Lett.* **2021**, *127*, 243602. [CrossRef]
34. Liedl, C.; Tebbenjohanns, F.; Bach, C.; Pucher, S.; Rauschenbeutel, A.; Schneeweiss, P. Observation of superradiant bursts in a cascaded quantum system. *Phys. Rev. X* **2024**, *14*, 011020. [CrossRef]
35. Ferioli, G.; Ferrier-Barbut, I.; Browaeys, A. Emergence of second-order coherence in the superradiant emission from a free-space atomic ensemble. *Phys. Rev. Lett.* **2025**, *134*, 153602. [CrossRef]
36. Bach, C.; Tebbenjohanns, F.; Liedl, C.; Schneeweiss, P.; Rauschenbeutel, A. Emergence of second-order coherence in superfluorescence. *Phys. Rev. Lett.* **2026**, *136*, 063402. [CrossRef]
37. Baumann, K.; Guerlin, C.; Brennecke, F.; Esslinger, T. Dicke quantum phase transition with a superfluid gas in an optical cavity. *Nature* **2010**, *464*, 1301–1306. [CrossRef]
38. Ferioli, G.; Glicenstein, A.; Ferrier-Barbut, I.; Browaeys, A. A non-equilibrium superradiant phase transition in free space. *Nat. Phys.* **2023**, *19*, 1345–1349. [CrossRef]
39. Braggio, C.; Chiossi, F.; Carugno, G.; Ortolan, A.; Ruoso, G. Spontaneous formation of a macroscopically extended coherent state. *Phys. Rev. Res.* **2020**, *2*, 033059. [CrossRef]
40. Chiossi, F.; Braggio, C.; Khanbekyan, A.; Carugno, G.; Ortolan, A.; Ruoso, G.; Calabrese, R.; Di Lieto, A.; Tomassetti, L.; Tonelli, M. Cascade superfluorescence in Er:YLF. *Phys. Rev. Res.* **2021**, *3*, 013138. [CrossRef]
41. Ariunbold, G.O.; Kash, M.M.; Sautenkov, V.A.; Li, H.; Rostovtsev, Y.V.; Welch, G.R.; Scully, M.O. Observation of picosecond superfluorescent pulses in rubidium atomic vapor pumped by 100-fs laser pulses. *Phys. Rev. A* **2010**, *82*, 043421. [CrossRef]
42. Ariunbold, G.O.; Sautenkov, V.A.; Scully, M.O. Temporal coherent control of superfluorescent pulses. *Opt. Lett.* **2012**, *37*, 2400–2402. [CrossRef]
43. Ariunbold, G.O.; Yang, W.; Sokolov, A.V.; Sautenkov, V.A.; Scully, M.O. Superradiance in a three-photon resonant medium. *Phys. Rev. A* **2012**, *85*, 023424. [CrossRef]
44. Thompson, J.V.; Ballmann, C.W.; Cai, H.; Yi, Z.; Rostovtsev, Y.V.; Sokolov, A.V.; Hemmer, P.; Zheltikov, A.M.; Ariunbold, G.O.; Scully, M.O. Pulsed cooperative backward emissions from non-degenerate atomic transitions in sodium. *New J. Phys.* **2014**, *16*, 103017. [CrossRef]
45. Ariunbold, G.O.; Sautenkov, V.A.; Scully, M.O. Ultrafast laser control of backward superfluorescence towards standoff sensing. *Appl. Phys. Lett.* **2014**, *104*, 021114. [CrossRef]
46. Ariunbold, G.O.; Sautenkov, V.A.; Li, H.; Murawski, R.K.; Wang, X.; Zhi, M.; Begzjav, T.; Sokolov, A.V.; Scully, M.O.; Rostovtsev, Y.V. Observations of ultrafast superfluorescent beatings in a cesium vapor excited by femtosecond laser pulses. *Phys. Lett. A* **2022**, *428*, 127945. [CrossRef]
47. Holzinger, R.; Rubies-Bigorda, O.; Yelin, S.F.; Ritsch, H. Symmetry-based efficient simulation of higher-order coherences in quantum many-body superradiance. *Phys. Rev. Res.* **2025**, *7*, 033203. [CrossRef]
48. Lee, C.T. Exact solutions of the superradiance master equation. I. Complete initial excitation. *Phys. Rev. A* **1977**, *15*, 2019–2029. [CrossRef]
49. Lee, C.T. Exact solution of the superradiance master equation. II. Arbitrary initial excitation. *Phys. Rev. A* **1977**, *16*, 301–312. [CrossRef]

50. Lee, C.T. Fluctuations in tipping angles and delay times of simple superfluorescence. *Appl. Phys. Lett.* **1982**, *41*, 821–823. [CrossRef]
51. R. Holzinger, C. Genes, A compact analytical solution of the Dicke superradiance master equation via residue calculus. *Z. Naturforsch. A* **2025**, *80*, 673–679. [CrossRef]
52. Holzinger, R.; Bassler, N.S.; Lyne, J.; Jimenez, F.G.; Gohsrich, J.T.; Genes, C. Solving Dicke superradiance analytically: A compendium of methods. *Phys. Rev. A* **2026**, *113*, 043718. [CrossRef]
53. Gumbel, E.J. *Statistics of Extremes*; Columbia University Press: New York, NY, USA, 1958.
54. Feller, W. *An Introduction to Probability Theory and Its Applications*, 3rd ed.; Wiley: New York, NY, USA, 1968; Volume 1.
55. Rényi, A. On the theory of order statistics. *Acta Math. Acad. Sci. Hung.* **1953**, *4*, 191–231. [CrossRef]
56. Vrehen, Q.H.F.; Schuurmans, M.F.H.; Polder, D. Superfluorescence: Macroscopic quantum fluctuations in the time domain. *Nature* **1980**, *285*, 70–71. [CrossRef]
57. Vrehen, Q.H.F.; der Weduwe, J.J. Quantum fluctuations in superfluorescence delay times. *Phys. Rev. A* **1981**, *24*, 2857–2860. [CrossRef]
58. Crubellier, A.; Liberman, S.; Pillet, P.; Schweighofer, M.G. Experimental study of quantum fluctuations of polarisation in superradiance. *J. Phys. B* **1981**, *14*, L177–L181. [CrossRef]
59. Holzinger, R.; Bassler, N.S.; Lyne, J.; Yelin, S.F.C.; Genes, C. Symbolic quantum-trajectory method for multichannel Dicke superradiance. *arXiv* **2025**, arXiv:2511.02390.
60. Eggenberger, F.; Pólya, G. Über die Statistik verketteter Vorgänge. *Z. Angew. Math. Mech.* **1923**, *3*, 279–289. [CrossRef]
61. Freedman, D.A. Bernard Friedman's urn. *Ann. Math. Stat.* **1965**, *36*, 956–970.
62. Bagchi, A.; Pal, A.K. Asymptotic normality in the generalized Pólya–Eggenberger urn model, with an application to computer data structures. *SIAM J. Algebr. Discret. Methods* **1985**, *6*, 394–405. [CrossRef]

Disclaimer/Publisher's Note: The statements, opinions and data contained in all publications are solely those of the individual author(s) and contributor(s) and not of MDPI and/or the editor(s). MDPI and/or the editor(s) disclaim responsibility for any injury to people or property resulting from any ideas, methods, instructions or products referred to in the content.